

# Image accuracy and quality test in rate constant depending on reconstruction algorithms with and without incorporating PSF and TOF in PET imaging

Yukito Maeda<sup>1,2</sup> · Nobuyuki Kudomi<sup>3</sup> · Hiroyuki Yamamoto<sup>3</sup> · Yuka Yamamoto<sup>4</sup> · Yoshihiro Nishiyama<sup>4</sup>

Received: 25 November 2014 / Accepted: 22 April 2015 / Published online: 6 May 2015  
© The Japanese Society of Nuclear Medicine 2015

## Abstract

**Objective** Positron emission tomography allows imaging of patho-physiological information as a form of rate constants from scanned and reconstructed dynamic image. Some reconstruction algorithms incorporated with time of flight and point spread function have been developed, and quantitative accuracy and quality in the image have been investigated. However, feasibility of the rate constants from the dynamic image has not been directly investigated. We investigated the accuracy and quality in the rate constant by scanning a phantom filled simultaneously with <sup>11</sup>C and <sup>18</sup>F.

**Method** We utilized a phantom filled with <sup>18</sup>F-F<sup>-</sup> solution in the main cylinder and with <sup>11</sup>C-flumazenil solution in seven sub-cylinders. The phantom was scanned by a Biograph mCT and the scanned data were reconstructed with FBP- and OSEM-based algorithms incorporating with and without TOF and/or PSF corrections. Decay rate images as kinetic rate constant were computed for all the

reconstructed images and quantitative accuracy and quality in the rate images were investigated.

**Results** The obtained decay rates were not significantly different from the reference values for both isotopes for all applied algorithms when noise on image was not large. Respective SD was smaller in OSEM with TOF in the <sup>11</sup>C-filled region.

**Conclusion** The present study suggests that OSEM incorporating with TOF provides reasonable quantitative accuracy and image quality regarding decay rates.

**Keywords** Feasibility test · Rate constant · Phantom · PET · Kinetic analysis

## Introduction

Positron emission tomography (PET) using radiotracers with quantitative analysis provides physiological information of organs as a form of rate constant(s) [1]. Quantitative accuracy and, in particular, image quality in PET image have been improved concerning PET devices and reconstruction algorithms [2], namely, advancement of reconstruction algorithms in imaging is remarkable in nuclear medicine field [3].

Several studies have demonstrated to characterize some reconstruction algorithms such as filtered back projection (FBP) and ordered-subsets expectation maximization (OSEM) [4–6]. Those studies showed that OSEM was advantageous than FBP in terms of image quality and resolution in cardiac study, and that was generally in good agreement with FBP in pixel value and subsequent estimated kinetic parameters.

Besides the development of the reconstruction algorithms, recently additional improvements have been

✉ Yukito Maeda  
yukito@med.kagawa-u.ac.jp

Nobuyuki Kudomi  
kudomi@med.kagawa-u.ac.jp

<sup>1</sup> Division of Social and Environmental Medicine, Graduate School of Medicine, Kagawa University, Miki-cho, Kagawa, Japan

<sup>2</sup> Department of Clinical Radiology, Kagawa University Hospital, Miki-cho, Kagawa, Japan

<sup>3</sup> Department of Medical Physics, Faculty of Medicine, Kagawa University, Miki-cho, Kagawa, Japan

<sup>4</sup> Department of Radiology, Faculty of Medicine, Kagawa University, Miki-cho, Kagawa, Japan

achieved by incorporating point spread function (PSF) and time-of-flight (TOF) techniques and those TOF and PSF have been implemented in some PET scanner software [7–9]. It was demonstrated that the incorporation with PSF allowed improvement in terms of spatial resolution and noise property [10, 11], implementation of TOF also improves image contrast and quality [12], and that combination of them improves small lesion detectability [13].

A number of studies have assessed the quantitative accuracy, spatial resolution and noise property of reconstruction algorithms with or without incorporating PSF and/or TOF. However, there are no studies assessing kinetic parameter estimation directly from FBP- and OSEM-based dynamic images in PET studies, though there are some studies comparing those between FBP and OSEM [3, 5].

In the present study, we tested accuracy of rate parameter and image quality by estimating decay rate of two known isotopes, i.e.,  $^{11}\text{C}$  with the decay constant:  $\lambda = 34.1 \times 10^{-3} \text{ min}^{-1}$  and  $^{18}\text{F}$  with  $\lambda = 6.31 \times 10^{-3} \text{ min}^{-1}$ , those were simultaneously filled in a phantom in separate regions.

## Materials and methods

### Phantom

A JSP model phantom (KYOTO KAGAKU CO., LTD, Kyoto, Japan) was used for the present study (Fig. 1a). The phantom was made with methyl methacrylate, was cylindrical shape with 99 mm in height and 200 and 210 mm in inner and outer diameters, respectively, and consisted of seven sub-cylinders with 30 and 36 mm in inner and outer diameters, respectively, i.e., 3 mm in width of the sub-

cylinder wall. One of sub-cylinders was at the center and the others were surrounding the central cylinder located 75 mm from the center of the phantom.

### PET experiments

The PET scanner used was Biograph mCT64-4R PET/CT system (Siemens Medical Solutions, Knoxville, TN, USA), containing LSO scintillation crystals. The scanner allows tomographic images with field of view (FOV) of 70.0 cm in diameter and 21.6 cm in axial length. The spatial resolution was 4.1 mm in full width at half maximum (FWHM) at 1 cm from the center of the FOV. The coincidence time window applied was 4.1 ns, and time resolution for TOF was 555 ps.

The phantom used was filled with  $^{18}\text{F}\text{-F}^-$  ion solution in the main part and with  $^{11}\text{C}$ -flumazenil in the all sub-cylinder regions, respectively. The phantom was set on a gantry of the PET scanner. Activity concentration of the solution each was 20 and 30 kBq/ml for  $^{18}\text{F}$  and  $^{11}\text{C}$ , respectively, at the start time of the PET scanning, so as to be the similar level in our routine clinical scanning. After CT scanning for attenuation correction, a list mode scan for 120 min was started in the 3-D list mode.

### Data processing

The list mode data collected were sorted to produce dynamic sinogram, with frame durations of 24 times 300 s, i.e., 120 min in total. Images were then reconstructed by the FBP and OSEM bases with or without incorporating TOF and PSF, without decay correction, including corrections for dead time, detectors normalization, CT-based attenuation and scatter (single scatter simulation method [14]) using the vendor software programs, namely, FBP, FBP with TOF (FBP + TOF), OSEM, OSEM with TOF (OSEM + TOF), OSEM with PSF (OSEM + PSF), OSEM with PSF and TOF (OSEM + PSF + TOF). For the OSEM and OSEM + PSF procedure, applied conditions were 3 iterations and 24 subsets, and for OSEM + TOF and OSEM + PSF + TOF, those were 3 iterations and 21 subsets, where 2 or 3 iterations were recommended in a previous study [15] and we fixed the number as 3 in the present study. For all the reconstruction procedure, filtering applied was Gaussian filter with 6 mm to compare the characteristics of the reconstruction algorithms in a same condition. The reconstructed images consisted of  $256 \times 256 \times 45$  matrix, with a pixel size of  $1.27 \text{ mm} \times 1.27 \text{ mm} \times 5 \text{ mm}$  and with 24 frames.

Decay rate was computed in a pixel-wise manner by fitting a single exponential function applying the basis function method (BFM) [16] as follows. For the one tissue compartment model, a tissue curve  $[C(t)]$  can be expressed as;

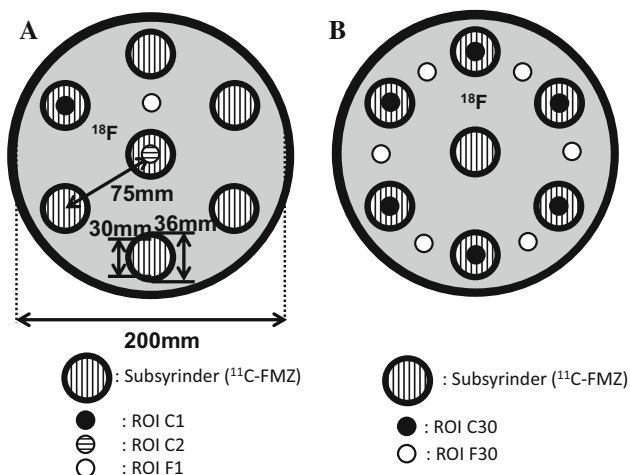


**Fig. 1** ROIs placed are also indicated (see text)

$$C(t) = K_1 \cdot A(t) \otimes \exp(-k_2 t) \quad (1)$$

where  $K_1$  and  $k_2$  are forward and backward transfer rate constants from blood to tissue, namely physiological parameter to be obtained in the kinetic analysis,  $A(t)$  is an input function, and  $\otimes$  denotes the convolution integral. The BFM applies linear least squares together with a discretized range of basis functions incorporating the nonlinearity and covering the expected physiological range. The corresponding basis function formed as:

$$F(k_2, t) = A(t) \otimes \exp(-k_2 t) \quad (2)$$

Then Eq. (1) can then be transformed for each basis function into a linear equation in  $K_1$  as:

$$C(t) = K_1 \cdot F(k_2, t) \quad (3)$$

Hence for fixed values of  $k_2$ ,  $K_1$  can be estimated using standard linear least squares. The  $k_2$  for which the residual sum of square is minimized is determined by a direct search and associated set of parameter values for this solutions: ( $K_1$ ,  $k_2$ ) are obtained. For the reasonable range of  $k_2$ , i.e.,  $0 < k_2 < 1.0 \text{ min}^{-1}$ , 10000 discrete values for  $k_2$  were found to be sufficient. For the present computation, the input function was determined to be the delta function, i.e.,  $\delta(0)$ , and the Eq. (1) becomes a simple exponential function. The computation was performed using all the reconstructed images, for 60 min starting at 0 min (first half) and start at 60 min (second half). Also, the decay rate was computed for 30 min duration starting at 0–90 min with every 10th min.

## Data analysis

Three circular regions of interest (ROI) with 12.7 mm in diameter were placed in 21st to 25th slices in the summed reconstruction image for all frames, two were placed at the center of the sub-cylinders at the top-left (C1) and central place (C2), namely, in the  $^{11}\text{C}$  regions and the other one was placed between them (F1), namely, in the  $^{18}\text{F}$  region (Fig. 1a). Circular ROIs with the same diameter were also placed in all the sub-cylinders except the central one in  $^{11}\text{C}$  region in the 21st to 25th slices (C30), namely 30 ROIs in total, and other 30 ROIs were placed between those sub-cylinders in  $^{18}\text{F}$  region (F30) (Fig. 1b).

Profiles of the cross-sectional distribution of the 23rd slice for the pixel value in summed images for first and second halves and decay rate for both the halves were extracted from top to bottom in the vertical direction at the horizontal 128th pixel. Mean ( $\pm$ SD) and coefficient of variation (CV) of summed pixel value and decay rate value were extracted from all the ROIs for all of the six reconstruction algorithms. For the two sets of ROIs of C30 and F30, mean values and CVs of decay rate were extracted for

30 ROIs and respective mean and SD were computed to test statistical significance between the algorithms. Paired  $t$  test was applied to compare the obtained values, and  $P < 0.05$  was considered statistically significant.

## Results

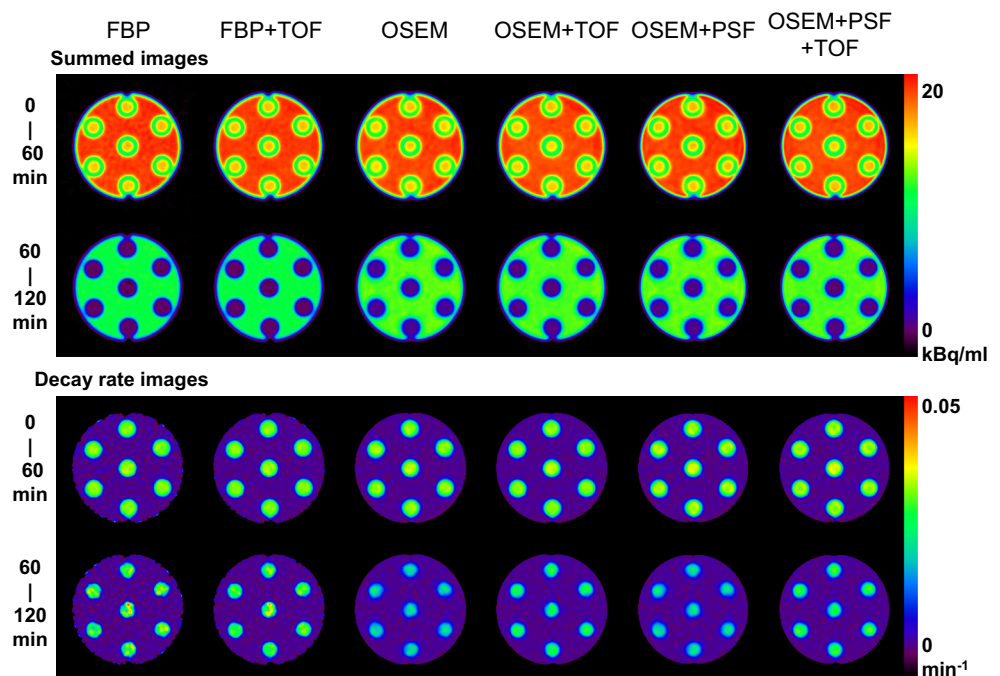
The summed and estimated decay rate images in the 23rd slice for all applied reconstruction algorithms are shown in Fig. 2. Both of the summed and decay rate images in the second half seem to be suffered from noise more in the FBP and FBP + TOF than the other OSEM-based images in the  $^{11}\text{C}$  regions. For all summed images, boundary part of sub-cylinder, i.e., cold part, seems lower value for all summed images in the first half, but the decay rate images, any lower rate cannot apparently be seen in that part. For the rate in  $^{11}\text{C}$  region, degree of error seems similar among the images from 0 to 60 min fitting; however, the degree of underestimation seems more in the images from 60 to 120 min, particularly in images with OSEM-based algorithm without incorporating TOF.

Profile of the cross-sectional distribution in the summed and estimated decay rate images are shown in Fig. 3. The boundary part of sub-cylinder shows lower value in all, particularly in FBP and FBP + TOF, summed images. For the decay rate, uniformity is more for OSEM-based summed images than that for both FBP-based images in the second half. The estimated decay rates were close to known physical decay constant in the  $^{18}\text{F}$  region in all the applied algorithms. In the  $^{11}\text{C}$  region, the decay rate was close for all the images from the first half, but underestimated from the second half, and degree of underestimation was more in the OSEM-based algorithms. At the boundary part, the decay rate gradually changes from  $^{11}\text{C}$  to  $^{18}\text{F}$  decay rates depending on a ratio of distance from the regions filled with those solutions.

The estimated rate from the 30-min duration data is shown in Fig. 4. The rate was reasonably identical to the reference values for  $^{11}\text{C}$  regions until the fitting start time was earlier than 40 min. Then, the rate was basically underestimated after that for OSEM without incorporating TOF. The underestimation is also seen for OSEM with TOF after 50 min though degree is less than the others.

In Table 1, the pixel-wise mean  $\pm$  SD and CV of summed images are summarized for the three ROIs of C1, C2 and F1. There were small differences in the mean values among the applied algorithms in the first half, but in the second, the means were larger for OSEM-based images than that for FBP-based. The CV, corresponding to noise level, was smaller in the FBP + TOF in the first half for C1 and C2, that in the FBP-based method was larger in the second half than that in OSEM-based images. The CV in C2, i.e., central sub-cylinder was larger than that in C1, i.e.,

**Fig. 2** Images of summed and decay rate for the six reconstruction algorithms. The algorithms applied were indicated at the top of images. The summed images were obtained by summing from 0 to 60 min (*upper*) and from 60 to 120 min (*lower*), respectively, and the decay rate images were from 0 to 60 min and 60 to 120 min, respectively



surrounding one for FBP-based methods, but that is similar in the OSEM-based methods.

Mean of estimated decay rate and respective CV are summarized in Table 2. The decay rate was close to the reference value for all estimated value for the first half. However, that seemed to be underestimated for the second half for  $^{11}\text{C}$  region. The CV was the smaller in OSEM with incorporating TOF for  $^{18}\text{F}$ . The CV in C2, i.e., central sub-cylinder was larger than that in C1, i.e., surrounding one for FBP-based methods, but that is basically similar in the first half and smaller in the second in the OSEM-based methods.

Figure 5 shows the mean  $\pm$  SD of means and CVs in each ROI of C30 and F30 for decay rate. For the mean of estimated rates, difference was not significant (95 % confidence level assuming the normal distribution) against the reference decay constant in the first half. For the CV, significant difference were found for all pairs of algorithms, except between FBP and the two of OSEM with PSF incorporated methods  $^{11}\text{C}$  for the first half, OSEM and the other OSEM-based methods  $^{11}\text{C}$  for the second half, and between OSEM + TOF and OSEM + PSF and between OSEM and the other OSEM incorporating PSF methods for  $^{18}\text{F}$  for the first half.

## Discussion

In the present study, we estimated the decay rates of  $^{11}\text{C}$  and  $^{18}\text{F}$  from dynamic images by scanning the phantom simultaneously filled with both of those tracer solutions

and by reconstructing the scanned data. The reconstruction algorithms applied were FBP- and OSEM-based methods with and without incorporating TOF and/or PSF, namely, FBP, FBP + TOF, OSEM, OSEM + TOF, OSEM + PSF and OSEM + PSF + TOF. The means of decay rate were not significantly different from the reference rate constant values for both isotopes for all applied methods in the first half, suggesting the applied reconstruction algorithms are reasonably acceptable regarding quantitative accuracy for kinetic analysis. For the image quality in the decay rate, CV was significantly smaller in OSEM + TOF. These findings suggest that the OSEM with incorporating TOF would provide reasonable quantitative accuracy and better image quality. Several studies have been already investigated quantitative accuracy and image quality regarding reconstruction algorithms with and without incorporating TOF and/or PSF [7–12]. Those studies only focused on pixel value in a reconstructed image, but not on physiological parameters after kinetic analysis, such as rate constants. Boellaard et al. has demonstrated to investigate accuracy of kinetic parameters in cardiac study, but compared accuracy of the parameters by an image-based method against blood sampling method between from FBP- and OSEM-based images. Lubberink et al. [5] also compared accuracy of the kinetic parameters from OSEM-based method against those by FBP method, but not test the accuracy directly. In the present study, we investigated quantitative accuracy and image quality in terms of reconstruction algorithms in a direct fashion, by estimating physical decay rates of isotopes of  $^{11}\text{C}$  ( $\lambda = 0.0341 \text{ min}^{-1}$ ) and  $^{18}\text{F}$  ( $\lambda = 0.00631 \text{ min}^{-1}$ ). We assumed that the



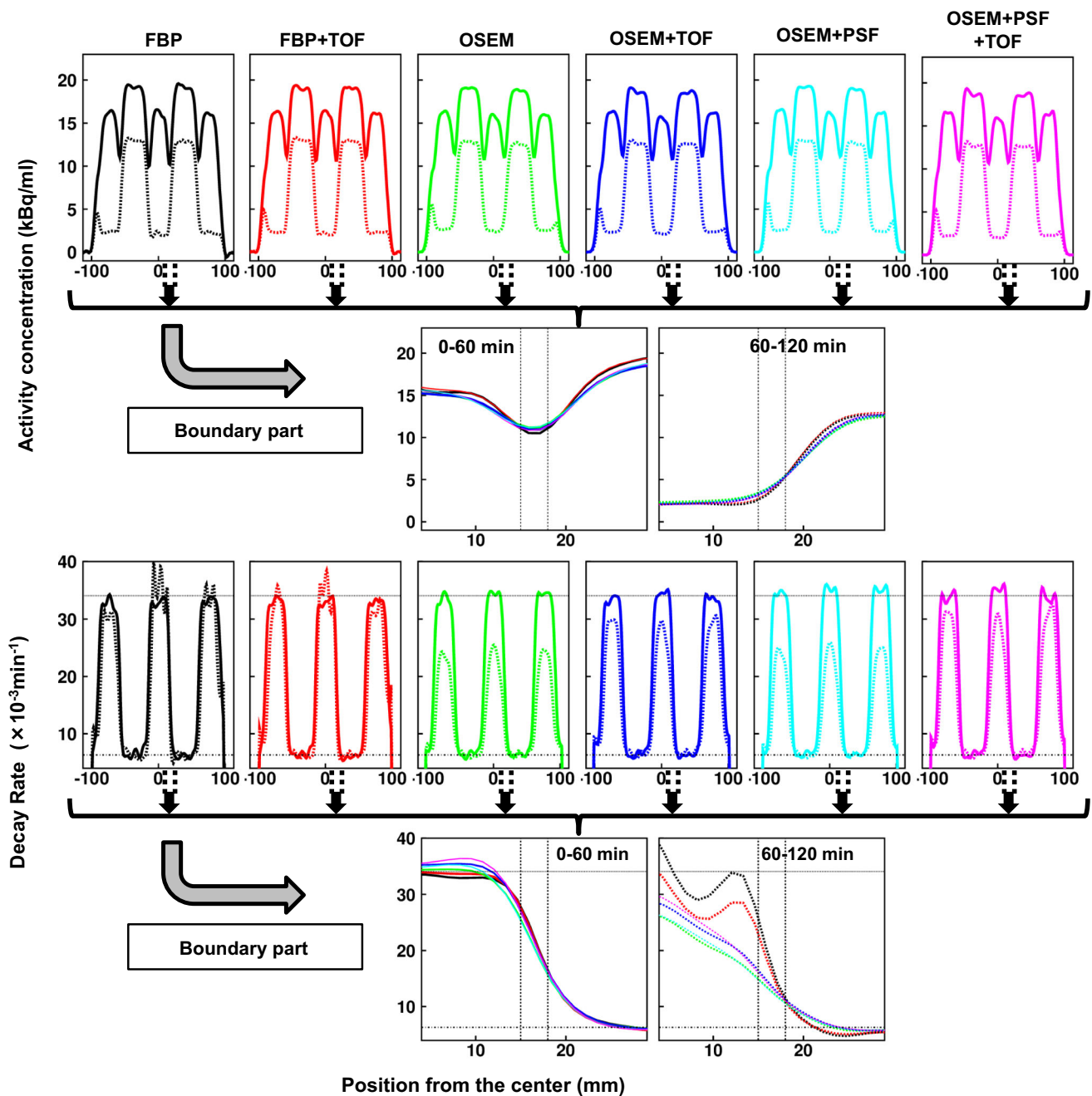


**Fig. 3** Profile of the cross-sectional distribution of pixel value in the summed images (*first row*) and decay rate (*third row*) for the six reconstruction algorithms and expansion of those at a boundary part (from 5 to 30 mm in pixel position, indicated as *arrow*) between  $^{11}\text{C}$  and  $^{18}\text{F}$  regions (*second and fourth rows*). In the top and third row, *solid and dashed lines* are profiles from 0 to 60 min and 60 to

120 min data, respectively. The respective *colors* in the figures represent the type of reconstruction indicated at the top of the first row figures. The *horizontal dashed lines* indicate decay constants of  $^{11}\text{C}$  and  $^{18}\text{F}$  in the decay rate profiles, and wall of boundary part is indicated with *vertical dashed lines*

physical characteristics of decay constant corresponds to a physiological kinetic parameter, in particular the decay constant of  $^{11}\text{C}$  is not very far to physiological transfer rate constants from brain tissue back to blood, i.e.,  $k_2$ , such as  $0.13 \pm 0.07 \text{ min}^{-1}$  and  $0.11 \pm 0.04 \text{ min}^{-1}$  for  $^{18}\text{F}$ -FDG in brain gray and white matter regions [17], respectively,

ranged from 0.099 to  $0.21 \text{ min}^{-1}$  for  $^{11}\text{C}$ -flumazenil in brain cortical regions [18], and  $0.10 \pm 0.07 \text{ min}^{-1}$  for  $^{18}\text{F}$ -FLT in glioma in brain [19].

For the boundary part of a sub-cylinder between  $^{11}\text{C}$  and  $^{18}\text{F}$ , namely cold part, the profile showed that the obtained pixel counts in both the FBP- and OSEM-based summed

images were smaller than surrounding hot part, but the value was not zero but biased. The bias would be due to spillover depending on filter size and spillover. The bias could be overcome by increasing the number of product of subset and iteration, but in the present case, width of 3 mm

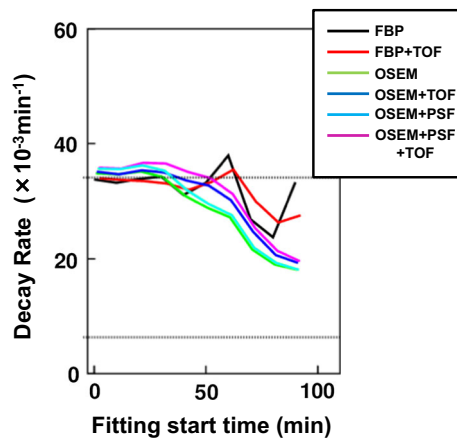


**Fig. 4** Estimated decay rates from 30-min duration data for C2 (with  $^{11}\text{C}$ ) region as a function of fitting start time

in cold part was too thin and that part was not clearly appeared by increasing the product, namely the number of iteration from 3 to 10 (data not shown). For that part, the decay rate seemed to appear as a ratio of estimated decay rates of two isotopes depending on distance to the regions of those solutions. In fact, the regression analysis indicated tight correlations (around 0.99 for all the methods) between the estimated decay rate and the position between 12 and 20 mm from the center of the phantom. The findings suggests that a kinetic parameter would be estimated as a mixture form of two or multiple rate constants at a boundary part where multiple rates contribute, and that the rate for the cold part would not be accurately estimated when the width of that part is thinner independent on the product of subset and iteration.

For computing the decay rate, we have applied the BFM, which is applied in some computation for physiological rate constants in the nuclear medicine field [16, 20–24]. Alternative for exponential fitting is a linear regression estimation on a semi-logarithmic plot. Difference between those two is in weighting, and might cause affect of accuracy of estimated parameter. For the two kinds of the

**Table 1** Mean  $\pm$  SD (kBq/ml) and respective coefficient of variation (%) in summed image

	FBP	FBP + TOF	OSEM	OSEM + TOF	OSEM + PSF	OSEM + TOF + PSF
0–60 min						
C1	15.95 $\pm$ 0.40 (2.52)	15.92 $\pm$ 0.40 (2.53)	15.58 $\pm$ 0.55 (3.54)	15.60 $\pm$ 0.50 (3.21)	15.77 $\pm$ 0.55 (3.96)	15.88 $\pm$ 0.57 (3.56)
C2	15.94 $\pm$ 0.48 (3.00)	15.94 $\pm$ 0.41 (2.55)	15.43 $\pm$ 0.51 (3.28)	15.24 $\pm$ 0.41 (2.70)	15.56 $\pm$ 0.62 (3.99)	15.38 $\pm$ 0.51 (3.31)
F1	19.35 $\pm$ 0.24 (1.24)	19.21 $\pm$ 0.20 (1.02)	19.06 $\pm$ 0.16 (0.83)	18.75 $\pm$ 0.19 (1.02)	19.16 $\pm$ 0.15 (0.76)	18.78 $\pm$ 0.18 (0.97)
60–120 min						
C1	1.87 $\pm$ 0.12 (6.62)	1.87 $\pm$ 0.08 (4.20)	2.60 $\pm$ 0.09 (3.56)	2.31 $\pm$ 0.06 (2.72)	2.51 $\pm$ 0.09 (3.49)	2.20 $\pm$ 0.05 (2.30)
C2	1.81 $\pm$ 0.13 (7.33)	1.81 $\pm$ 0.10 (5.62)	2.49 $\pm$ 0.09 (3.58)	2.18 $\pm$ 0.06 (2.82)	2.39 $\pm$ 0.07 (3.13)	2.05 $\pm$ 0.05 (2.43)
F1	11.89 $\pm$ 0.15 (1.02)	11.82 $\pm$ 0.12 (1.00)	12.90 $\pm$ 0.12 (0.92)	12.74 $\pm$ 0.12 (0.97)	12.96 $\pm$ 0.10 (0.80)	12.75 $\pm$ 0.12 (0.97)

The summed durations were from 0 to 60 min and 60 to 120 min, respectively. The ROI placed were C1 and C2 filled with  $^{11}\text{C}$ , and F1 with  $^{18}\text{F}$  regions (see Fig. 1), respectively

**Table 2** Mean  $\pm$  SD ( $10^{-3} \text{ min}^{-1}$ ) and respective coefficient of variation (%) of decay rate for ROIs in C1 and C2 filled with  $^{11}\text{C}$  ( $\lambda = 34.1 \times 10^{-3} \text{ min}^{-1}$ ), and F1 with  $^{18}\text{F}$  ( $\lambda = 6.31 \times 10^{-3} \text{ min}^{-1}$ ) regions (see Fig. 1), respectively

	FBP	FBP + TOF	OSEM	OSEM + TOF	OSEM + PSF	OSEM + TOF + PSF
0–60 min						
C1	33.85 $\pm$ 0.78 (2.3)	33.67 $\pm$ 0.53 (1.6)	34.39 $\pm$ 0.68 (2.0)	33.73 $\pm$ 0.36 (1.1)	35.07 $\pm$ 0.76 (2.2)	34.28 $\pm$ 0.65 (1.8)
C2	33.61 $\pm$ 1.02 (3.1)	33.69 $\pm$ 0.88 (2.6)	34.73 $\pm$ 0.68 (2.0)	35.02 $\pm$ 0.63 (1.8)	35.62 $\pm$ 0.67 (1.9)	35.94 $\pm$ 0.77 (2.2)
F1	6.41 $\pm$ 0.55 (8.7)	6.35 $\pm$ 0.42 (6.6)	6.45 $\pm$ 0.41 (6.4)	6.45 $\pm$ 0.38 (5.9)	6.45 $\pm$ 0.36 (5.6)	6.44 $\pm$ 0.37 (5.6)
60–120 min						
C1	30.24 $\pm$ 3.56 (11.8)	30.24 $\pm$ 2.42 (8.0)	22.49 $\pm$ 2.08 (9.3)	27.28 $\pm$ 2.33 (8.5)	23.03 $\pm$ 2.08 (9.1)	28.68 $\pm$ 2.58 (9.0)
C2	32.72 $\pm$ 4.67 (14.3)	32.45 $\pm$ 4.00 (12.3)	22.93 $\pm$ 1.50 (6.5)	25.97 $\pm$ 1.90 (7.3)	23.26 $\pm$ 1.52 (6.6)	26.86 $\pm$ 2.00 (7.4)
F1	6.33 $\pm$ 0.54 (8.5)	6.41 $\pm$ 0.44 (6.9)	6.39 $\pm$ 0.47 (7.4)	6.54 $\pm$ 0.44 (6.8)	6.40 $\pm$ 0.46 (7.1)	6.54 $\pm$ 0.44 (6.7)

The rates were obtained from 0 to 60 min and 60 to 120 min durations, respectively

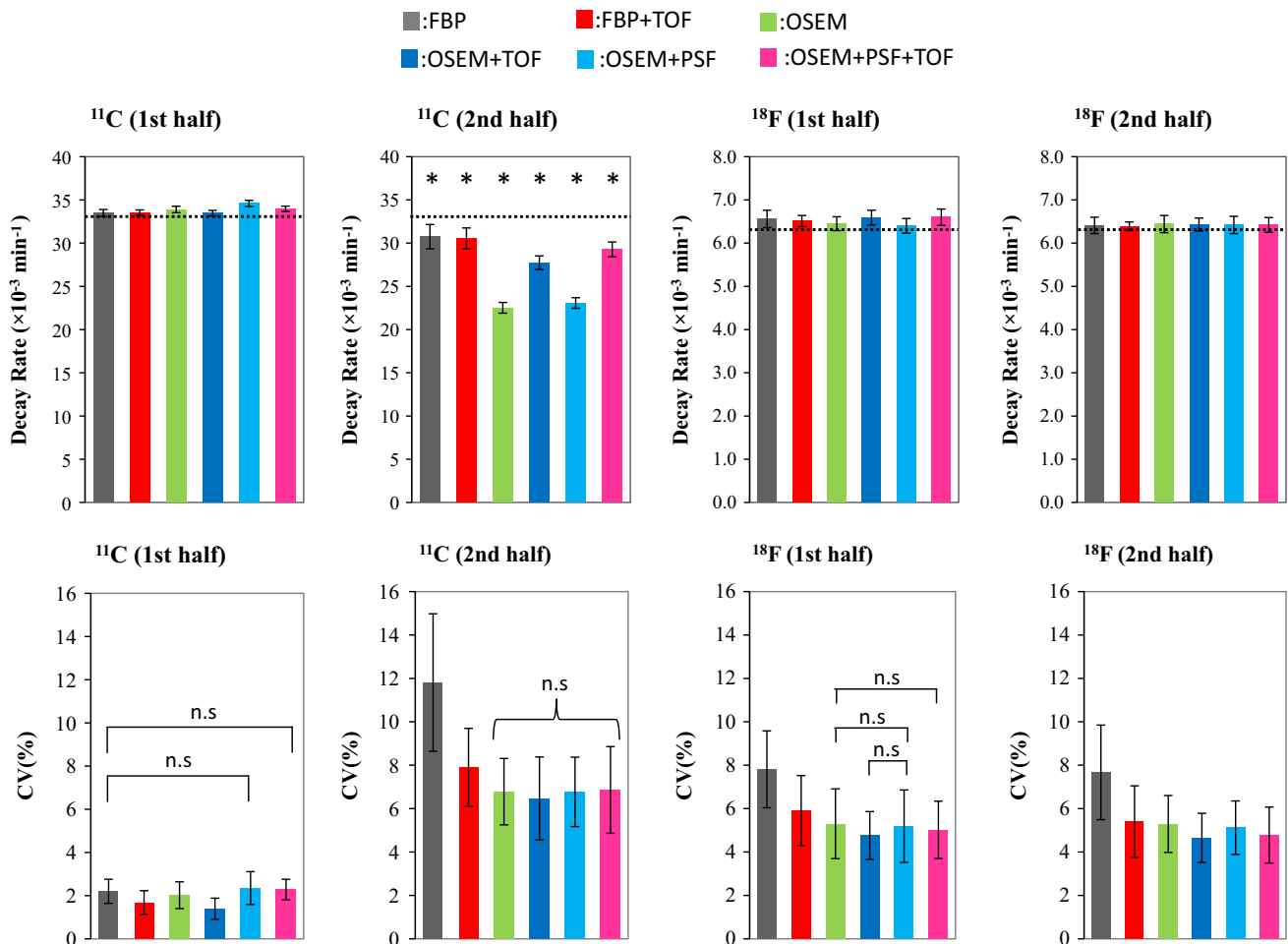


**Fig. 5** Mean (bar graph) and respective SD (error bar) obtained from mean ( $\text{min}^{-1}$ ) and CV (%) values of decay rate for set of ROIs of C30 and F30. The values were obtained from 0 to 60 min (first

half) and 60–120 min (second half) durations, respectively. \* and n.s. indicate that the difference was significant and not significant, respectively

fitting methods, we compared obtained decay rate values in our preliminary study, and these were no significant differences in estimated rates except the rates in  $^{11}\text{C}$  region from FBP and FBP + TOF when noise, i.e., CV, in summed image was larger.

The FBP is the conventionally applied reconstruction algorithm in PET imaging. As has been demonstrated in previous studies, image quality is poorer due to low signal-to-noise ratio, and the OSEM method was developed and introduced to overcome that problem [4, 6, 25, 26]. The present study also showed that the noise level was larger in both FBP than that in the other methods in summed and subsequent decay rate images, particularly in the second half. For quantitative accuracy in all the methods, the estimated decay rates were not significantly different to the reference values for both  $^{11}\text{C}$  and  $^{18}\text{F}$  when data in the first half was applied; however, when applied second half, the decay rate in the  $^{11}\text{C}$  region was significantly underestimated. The underestimation might be due to affect of

spillover, namely the affect is larger when activity concentration from adjacent region is larger. In fact, we found that a time activity curve at a pixel at center in the ROI C2 was higher in the late phase (>60 min) than an extrapolated fitted curve during 0–60 min for the OSEM-based images, and the difference between the time activity curve at center and fitted curve was consistent to a curve at outside, i.e., a pixel at 15 mm from the edge of the main cylinder. For degree of the spillover for the pixel at the 15 mm outside, activity level was consistent to zero for FBP-based images, and the degree was the most for the OSEM image and that was twofold than that of OSEM + TOF, three times than OSEM + PSF, and four times than OSEM + TOF + PSF. As a whole, the overestimation due to spillover would cause smaller estimation of rates after 40 min in Fig. 4. However, the degree was less when TOF was incorporated in the OSEM method, which might contribute to improve image quality. The finding would suggest usefulness of TOF method. For the rate in FBP in Fig. 4, the degree of

underestimation was not stable. Our preliminary simulation showed that the BFM derives overestimation in the decay rate when the level of noise is larger than 15 % in the 60-min summed image, and that the rates are around 2 % overestimated when the noise level is from 5 to 10 %. This fact suggests that the unstable estimation in FBP would be due to noise on image.

It was suggested that, when ratio of activity concentration at edge was larger, namely, the ratio was around 1:8, an overshoot due to Gibbs artifact occurred with incorporating PSF [27, 28]. In this study, however, at the boundary part of a sub-cylinder between  $^{11}\text{C}$  and  $^{18}\text{F}$  regions, any overshoot has not apparently been seen with or without PSF incorporated images. This could be due to smaller ratio of the activity concentration in the present condition, namely 2:3 for  $^{18}\text{F}$  and  $^{11}\text{C}$ , respectively, at the scan start time and larger size of cylinder of 30 mm in diameter. Subsequently, there were also no apparent such affect in the decay rate. Further study is required to make reveal the effect to the decay rate.

Limitations of the present study are (1) the study only estimated decay rate corresponding to physiologically backward transfer rate, meaning accuracy of forward rates were not directly tested (2) the width of boundary between  $^{11}\text{C}$  and  $^{18}\text{F}$  was not thin enough, i.e., 3 mm to simulate physiological difference of rate constants at adjacent regions, and (3) an affect of overshoot, which would occur when a difference of activity concentration at a boundary part is large, has not been made reveal regarding kinetic parameters.

In conclusion, the present study made reveal that the accuracy and image quality in the rate images, and suggested that the reconstruction algorithm of OSEM incorporating TOF would provide reasonable quantitative accuracy and image quality in estimating a rate constant.

**Acknowledgments** The authors thank the staff at Department of Clinical Radiology in our University Hospital and at Department of Medical Physics in our University. The work of NK was supported by the Ministry of Education, Science, Sports and Culture of Japan, a grant-in-aid for JSPS KAKENHI (C) Grant number 26460728 (2014–2017).

## References

1. Watabe H, Ikoma Y, Kimura Y, Naganawa M, Shidahara M. PET kinetic analysis—compartmental model. *Ann Nucl Med*. 2006;20:583–8.
2. Peng H, Levin CS. Recent developments in PET instrumentation. *Curr Pharm Biotechnol*. 2010;11:555–71.
3. Tong S, Alessio AM, Kinahan PE. Image reconstruction for PET/CT scanners: past achievements and future challenges. *Imaging Med*. 2010;2:529–45.
4. Boellaard R, van Lingem A, Lammertsma AA. Experimental and clinical evaluation of iterative reconstruction (OSEM) in dynamic PET: quantitative characteristics and effects on kinetic modeling. *J Nucl Med*. 2001;42:808–17.
5. Lubberink M, Boellaard R, van der Weerd AP, Visser FC, Lammertsma AA. Quantitative comparison of analytic and iterative reconstruction methods in 2- and 3-dimensional dynamic cardiac 18F-FDG PET. *J Nucl Med*. 2004;45:2008–15.
6. Søndergaard HM, Boisen K, Böttcher M, Schmitz O, Nielsen TT, Bøtker HE, et al. Evaluation of iterative reconstruction (OSEM) versus filtered back-projection for the assessment of myocardial glucose uptake and myocardial perfusion using dynamic PET. *Eur J Nucl Med Mol Imaging*. 2007;34:320–9.
7. Surti S, Kuhn A, Werner ME, Perkins AE, Kolthammer J, Karp JS. Performance of Philips Gemini TF PET/CT scanner with special consideration for its time-of-flight imaging capabilities. *Nucl Med*. 2007;48:471–80.
8. Jakoby BW, Bercier Y, Conti M, Casey ME, Bendriem B, Townsend DW. Physical and clinical performance of the mCT time-of-flight PET/CT scanner. *Phys Med Biol*. 2011;56:2375.
9. Bettinardi V, Presotto L, Rapisarda E, Picchio M, Gianolli L, Gilardi MC. Physical performance of the new hybrid PET/CT discovery-690. *Med Phys*. 2011;38:5394–441.
10. Panin VY, Kehren F, Michel C, Casey M. Fully 3-D PET reconstruction with system matrix derived from point source measurements. *IEEE Trans Med Imaging*. 2006;25:907–21.
11. Tong S, Alessio AM, Kinahan PE. Noise and signal properties in PSF-based fully 3D PET image reconstruction: an experimental evaluation. *Phys Med Biol*. 2010;55:1453–73.
12. Lois C, Jakoby BW, Long MJ, Hubner KF, Barker DW, Casey ME, et al. An assessment of the impact of incorporating time-of-flight (TOF) information into clinical PET/CT imaging. *J Nucl Med*. 2010;51:237–45.
13. Akamatsu G, Mitsumoto K, Taniguchi T, Tsutsui Y, Baba S, Sasaki M. Influences of point-spread function and time-of-flight reconstructions on standardized uptake value of lymph node metastases in FDG-PET. *Eur J Radiol*. 2014;83:226–30.
14. Watson CC. New, faster, image-based scatter correction for 3D PET. *IEEE Trans Nucl Sci*. 2000;47:1587–94.
15. Akamatsu G, Ishikawa K, Mitsumoto K, Taniguchi T, Ohya N, Baba S, et al. Improvement in PET/CT image quality with a combination of point-spread function and time-of-flight in relation to reconstruction parameters. *J Nucl Med*. 2012;53:1716–22.
16. Koeppe RA, Holden JE, Ip WR. Performance comparison of parameter estimation techniques for the quantitation of local cerebral blood flow by dynamic positron computed tomography. *J Cereb Blood Flow Metab*. 1985;5:224–34.
17. Phelps ME, Huang SC, Hoffman EJ, Selin C, Sokoloff L, Kuhl DE. Tomographic measurement of local cerebral glucose metabolic rate in humans with (F-18) 2-fluoro-2-deoxy-D-glucose: validation of method. *Ann Neurol*. 1979;6:371–88.
18. Koeppe RA, Holthoff VA, Frey KA, Kilbourn MR, Kuhl DE. Compartmental analysis of [ $^{11}\text{C}$ ]flumazenil kinetics for the estimation of ligand transport rate and receptor distribution using positron emission tomography. *J Cereb Blood Flow Metab*. 1991;11:735–44.
19. Schiepers C, Dahlbom M, Chen W, Cloughesy T, Czernin J, Phelps ME, et al. Kinetics of 3'-deoxy-3'-18F-fluorothymidine during treatment monitoring of recurrent high-grade glioma. *J Nucl Med*. 2010;51:720–7.
20. Gunn RN, Lammertsma AA, Hume SP, Cunningham VJ. Parametric imaging of ligand-receptor binding in PET using a simplified reference region model. *Neuroimage*. 1997;6:279–87.
21. Watabe H, Jino H, Kawachi N, Teramoto N, Hayashi T, Ohta Y, Iida H. Parametric imaging of myocardial blood flow with 15O-water and PET using the basis function method. *J Nucl Med*. 2005;46:1219–24.



22. Boellaard R, Knaapen P, Rijbroek A, Luurtsema GJ, Lammertsma AA. Evaluation of basis function and linear least squares methods for generating parametric blood flow images using  $^{15}\text{O}$ -water and positron emission tomography. *Mol Imaging Biol.* 2005;7:273–85.
23. Kudomi N, Koivuviita N, Liukko KE, Oikonen VJ, Tolvanen T, Iida H, et al. Parametric renal blood flow imaging using  $^{15}\text{O}$  and PET. *Eur J Nucl Med Mol Imaging.* 2009;36:683–91.
24. Kudomi N, Hirano Y, Koshino K, Hayashi T, Watabe H, Fukushima K, et al. Rapid quantitative CBF and  $\text{CMRO}_2$  measurements from a single PET scan with sequential administration of dual  $^{15}\text{O}$ -labeled tracers. *J Cereb Blood Flow Metab.* 2013;33:440–8.
25. Hudson HM, Larkin RS. Accelerated image-reconstruction using ordered subsets of projection data. *IEEE Trans Med Imaging.* 1994;13:601–9.
26. Liow JS, Strother SC, Rehm K, Rottenberg DA. Improved resolution for PET volume imaging through three-dimensional iterative reconstruction. *J Nucl Med.* 1997;38:1623–31.
27. Bai B, Esser PD. The effect of edge artifacts on quantification of positron emission tomography. In: *IEEE nuclear science symposium and medical imaging conference record.* 2010; pp 2263–6.
28. Nakamura A, Tanizaki Y, Takeuchi M, Ito S, Sano Y, Sato M, et al. Impact of point spread function correction in standardized uptake value quantitation for positron emission tomography images: a study based on phantom experiments and clinical images. *Nihon Hoshasen Gijutsu Gakkai Zasshi.* 2014;70:542–8.